Nuclear Fusion **XX** (2019) XXXXXX https://doi.org/XXXX/XXXX

High Performance Double-null Plasmas Under Radiating Divertor and Mantle Scenarios on DIII-D

T.W. Petrie[1], B.A. Grierson[2], T. Osborne[1], C.C. Petty[1], F. Turco[3], S.L. Allen[4], M.E. Fenstermacher[4], J.R. Ferron[1], H. Guo[1], E.T. Hinson[5], R.J. La Haye[1], C.J. Lasnier[4], A.W. Leonard[1], A.G. McLean[4], B. Victor[4], H. Wang[6], and J.G. Watkins[7]

[1] General Atomics, P.O. Box 85608, San Diego, CA 92186-5608, USA.
[2] Princeton Plasma Physics Laboratory, P.O. Box 451, Princeton, NJ 08540
[3] Columbia University, New York, NY 10027, USA.
[4] Lawrence Livermore National Laboratory, Livermore, CA 94550, USA.
[5] University of Wisconsin, Madison, WI, USA.
[6] Oak Ridge Associated Universities, Oak Ridge, Tennessee, USA
[7] Sandia National Laboratories, P.O. Box 969, Livermore, CA 94551, USA

E-mail: petrie@fusion.gat.com

Received xxxxxx
Accepted for publication xxxxxx
Published xxxxxx

Abstract

Experiments to combine a radiating divertor or mantle with high power, high β_N plasma operation have successfully reduced the divertor heat flux by 40% but have also encountered several challenging problems. For example, injecting either neon or argon seed impurities have led both to significant fuel dilution of the core plasma and to the emergence of harmful tearing mode activity which compromised plasma beta and energy confinement time. Increased divertor closure resulted in more effective control over the injected seed impurity inventory, although it was also observed that small radial variations in the placement of the outer separatrix strike point within the DIII-D "closed" divertor could lead to clear differences in the impurity build-up inside the core plasma. Active particle pumping of argon seed impurities through the divertor leg on the high-field side of a double-null divertor configuration showed little effect on seed impurity inventory and only modest control over the deuterium fuel inventory. Typically, 80% or greater of injected argon was removed by the corresponding cryo-pump on the low-field (outboard) side of that divertor, with the remaining argon being removed by the outboard cryo-pump from the opposite divertor. For single-null divertor cases, the contribution of the inner (high-field) cryo-pump to impurity and main-ion control appears to be complicated by the levels of divertor recycling and degree of divertor detachment. In general, divertor design that impedes the escape of seed impurities, plasma shaping that allows a higher stability limit, and electron cyclotron deposition profiles that prevent tearing mode onset and impede impurity accumulation in the core are under consideration for addressing the issues presented in this paper.

PACS: 52.55.Fa, 52.55.Tn, 52.55.Rk, 28.52.Cx

 © xxxx IOP Publishing Ltd

1. Introduction

Future tokamaks having elevated power exhaust face simultaneous requirements to avoid damaging power loads at their divertor targets, to maintain desirable high-performance plasma metrics, e.g., elevated energy confinement time τ_E and low plasma dilution, and to sustain adequate pumping for fuel and impurity particle control. Two potential solutions for achieving these goals are (1) the radiating "mantle" and (2) the radiating divertor, such as described in Refs. 1-8. In the latter, "seed" impurities are injected directly into the divertor, where these impurities can radiate significant fractions of the plasma-conducted power before it reaches the divertor surfaces. In the former, seed impurities accumulate in the pedestal region, resulting in a strong increase in radiative emissivity; due to the relatively large volume of the pedestal, radiated power from the main plasma is increased and power flow into the scrape-off layer SOL (and ultimately onto the divertor targets) is reduced. This study identifies issues that may impede the effectiveness of either approach during high power, high performance double-null divertor (DND) or single-null divertor (SND) plasma operation.

In section 2, the experimental arrangement and representative plasma parameters are presented. In section 3.1, we show how candidate seed impurities, such as neon or argon, are inadequate for radiating mantle operation at low to moderate density in DIII-D, leading instead to unacceptable fuel dilution in the highly powered, high normalized beta (β_N) plasmas considered in this paper. In section 3.2, impurity injection, whether neon or argon, is shown to lead to the onset of harmful tearing mode activity. Two additional topics that could affect fuel dilution and tearing mode activity are also presented. In section 3.3, we discuss how increased divertor closure can lead to better deuterium and seed impurity pumping in both SND and DND plasmas. Finally, in section 3.4, the role of an inner divertor pump in controlling argon and deuterium inventory in DND and SND configurations is evaluated. In section 4, we offer interim conclusions and point out directions for future research.

2. Experimental arrangement

We exploit the plasma shaping capabilities of DIII-D in producing the high triangularity, DND and SND shapes that are generally associated with elevated energy confinement time (τ_E) and β_N [9]. Figure 1 shows examples of both (a) the lower-biased and (b) the upper-biased DNDs used in this study; the lower- and upper-biased SNDs discussed in this paper are similarly situated. These plasmas are characterized (1) by the ion B x ∇B drift always directed away from their primary (i.e., main) divertor, (2) by particle pumping of deuterium and seed impurities from a maximum of three poloidal divertor locations, and (3) by D_2 gas injection from the low-field side and seed impurity injection capability from locations in either private flux region and from a non-divertor low-field side location (Fig. 1). In subsequent discussion, the upper divertor is referred to as "closed" and the lower divertor as "open". Note that the main difference between "closed" and "open" is that the latter does not have an inner baffle.

The high-performance ELMing plasmas used in these experiments are based on the 'steady state' hybrid scenario that used strong central current drive and bootstrap current to achieve zero loop voltage [10,11]. Here, the 'hybrid' regime refers to a stationary, high performance H-mode scenario that has higher confinement and greater stability to the 2/1 tearing mode than the conventional H-mode regime [12,13]. Representative plasma parameters were: normalized energy confinement $H_{98} = 1.4 - 1.7$, $\beta_N \geq 3$, plasma current $I_P \cong 1.0\ \mathrm{MA}$, $B_T = 1.9\ \mathrm{T}$, safety factor at the 95% flux surface $q_{95} \cong 6.0$, and total power input $P_{IN} \cong 12 - 15\ \mathrm{MW}$, where applied electron cyclotron heating (ECH) at 110 GHz with X-mode polarization provided plasma heating of up to 3.5 MW. Concerns over ECH cutoff/reflection limited the line-averaged density to $\leq 6 \times 10^{19}\mathrm{m}^{-3}$ (or $\approx$ 60% of the Greenwald density). Furthermore, to avoid exceeding ECH cutoff density, the location of ECH deposition used in this study was approximately half-way between the magnetic center and the plasma edge, i.e., normalized radius $\rho = 0.40 - 0.45$. While an earlier study found that this location results in somewhat more peaked impurity density profiles in DIII-D than if deposition were nearer the plasma center, e.g., at $\rho = 0.2$, plasma performance in terms of achievable β_N and H_{98} was unaffected [14].

Since the interior of the DIII-D vessel is protected by graphite tiles, carbon was the main intrinsic impurity. The injected "seed" species were the relatively low-Z recycling neon and medium-Z recycling argon. Both seed impurities were effective in reducing divertor heat flux on DIII-D in previous radiating divertor experiments, e.g., Ref. 15. Heat flux measurements in both divertors were based on infrared (IR) camera measurements. Two Penning gauges that measure neutral deuterium pressure, as well as neutral neon or argon pressures, are located inside the plenums housing the two outer divertor pumps. No Penning gauge was available for the upper inner pump. Electron density and temperature at the divertor targets were determined from fixed Langmuir probe measurements, while upstream and core densities and temperatures were based on Thomson scattering. The radial density profiles of the seed neon and argon impurities, in addition to the intrinsic carbon impurities, were based on charge-exchange recombination (CER) measurements.

3. Results

3.1 Effect of impurity selections on fuel dilution at high-power in near-DNDs

While significant fuel dilution in tokamak plasmas can exist under a variety of operating conditions involving impurity injection, fuel dilution can be particularly acute in DIII-D DND plasmas at very high power input. "Fuel dilution" is defined as n_D/n_e, where n_D and n_e are the deuterium fuel density and electron density in the main plasma, respectively; the lower this ratio, the more contaminated the plasma. In this section, we show that reducing divertor heat flux by impurity injection by only a modest amount resulted in unacceptable dilution.

An argon-based radiating mantle is compared with a neon-based radiating mantle in a lower-biased DND, where the seed impurities were injected from the low-field (non-divertor) location, as shown in Fig. 1. Both cases are characterized by the *same* 40% reduction in peak divertor heat flux, i.e., from 4.5 MW/m^2 to 2.6 MW/m^2. Both cases were identically prepared up to the point of impurity injection and had the same initial values of $\beta_N \cong 3.$, $H_{98} \cong 1.5$, and power input $\cong 14.7$ MW; these shots were run at moderate densities, i.e., Greenwald fractions of $\approx 0.5 - 0.6$. Central electron and ion temperatures at the plasma center for both argon and neon cases were $\cong$ 4 keV and $\cong$ 6 keV, respectively. A "control" case that had no impurity injection was also prepared in the same manner.

The radial density profiles for neon and argon, as based on charge-exchange recombination (CER) analyses for Ne^{10+} and Ar^{16+} and augmented by STRAHL [16] impurity transport code and bolometric analyses, are shown in Figs. 2(a,b). Also shown in Figs. 2(a,b) are the electron density profiles for each case. In the neon injection case, the neon profile was only slightly more peaked than its electron profile. However, in the argon injection case, the argon profile was considerably more peaked than its electron density profile. Also shown in Fig. 2(b) are the three argon charge states almost entirely responsible for the argon profile between $\rho = 0$ and $\rho = 0.7$. Because carbon and neon are both low-Z, the "peakedness" of the intrinsic carbon impurity profiles in both neon or argon injection cases were found to approximately match that of neon. That the profile of the high-Z impurity (argon) was much more peaked than that of the low-Z impurity (neon) would be expected, based on neoclassical transport of impurities, as demonstrated by Hirshman and Sigmar [17]. While an assessment of the neoclassical (and turbulent) particle transport responsible for this result is ongoing, the above results resemble recent studies of high-Z impurity transport in hybrid plasmas in JET [18]. In addition, other tokamaks have reported similar impurity ion behaviors between ECH applied on-axis and off-axis, e.g., tungsten in ASDEX-U H-mode plasmas [19] and argon in KSTAR L-mode plasmas [20]. Interestingly, central ECH was not even necessary for low-Z helium cases, since there was no evidence of central peaking of the helium density profile even in the presence of a central source [21].

The fuel dilution (n_D/n_e) for the neon-seeding and argon-seeding cases, as well as for the "control" case is shown in Table 1 for a central plasma location (ρ=0) and for a location approximately half-way to the edge (ρ=0.6). While both argon and neon cases indicate severe fuel dilution, particularly in the central plasma regions, fuel dilution in the neon case was far more pronounced. This was due largely to more neon required to match the heat flux reduction provided by argon, since neon has a lower cooling rate per neon ion than argon in the temperature ranges of interest, i.e., ≤40eV in the divertor and greater than ≈800 eV in the pedestal/core. Surprisingly, even in the control case, the carbon accumulation in the main plasma was also significant and led to noticeable fuel dilution, though not nearly as severe as that of the neon and argon cases. In the control case, carbon continued to accumulate in the main plasma up to the end of the "control" discharge; this carbon accumulation was due to SOL plasma interaction with the graphite tiles near the lower pump entrance and has been observed to be particularly severe in low and moderate density, highly powered discharges during long-pulses [22].

Figure 2(c) indicates that the radiative emissivities for neon and argon have a pronounced peaking near the plasma edge (i.e., the "mantle"). In large part, this peaking accounts for the nearly factor of two increase in the total radiated power from the main plasma relative to the control case. Since the argon near the plasma center was not completely ionized, as indicated in Fig. 2(b), both argon line radiation and bremsstrahlung contributed to the pronounced peaking observed in the on-axis emissivity. However, neon was completely ionized on-axis, so that bremsstrahlung was the dominant contributor to on-axis emissivity and lower on-axis peaking relative to argon was the result. We note that bolometric tomography used in the above analyses indicated that localized radiative emissivity near the X-points for these low to moderate density DND cases was absent.

In general, we found highly powered DND radiating mantle plasmas at modest density required significant impurity concentrations for even modest reduction in divertor heat flux, leading to significant fuel dilution. Operating these hybrid plasmas at higher density, while at the same time directing ECH deposition closer to the central plasma in order to minimize impurity peaking, would likely be very helpful in making this contamination problem more manageable. At present, however, this is not possible due to the hardware limits mentioned earlier in section 2.

3.2 Effect of tearing modes on confinement in high-power high-performance radiating mantle and divertor plasmas

The onset of tearing mode activity in high β_N plasmas was correlated with impurity injection and resulted in significant decreases in important plasma performance characteristics, such as normalized plasma beta β_N. To show this, we return

to the three shots discussed above in section 3.1. Figures 3(a1, b1, and c1) show MHD spectrograms for the control shot, the neon-seeded shot, and the argon-seeded shot, respectively. Each of the three shots had a m=4/n=2 mode (yellow) initially present. For the control case (Fig. 3(a1)), this 4/2 mode remained present all during the time interval of interest, i.e., between 2.5 s (after steady plasma operation was reached) and 4.8 s (shortly before steady plasma operation was terminated); the onset of other MHD modes was not observed during this interval. However, the spectrograms for plasmas in the neon (Fig. 3(b1)) and argon cases (Fig. 3(c1)) showed less benign 5/2 and 3/1 tearing modes emerging during impurity injection, the 5/2 mode (violet) starting ≈ 1 second after injection began and the 3/1 mode (red) at roughly one second after that. The tearing modes in these hybrid discharges evolved slightly differently those from previous experience due largely to differences in the deposition location of the ECH. The hybrid discharges discussed in this paper used off-axis ECH injection and were more prone to a relatively benign m=4/n=2 tearing mode over the time interval of interest, while the m=3/n=2 or m=5/n=2 tearing modes, which were more common in previous published work [11,12], had more centrally-directed ECH deposition.

The onset of each of these tearing modes adversely affected the plasma β_N in some degree. In principle, this drop in β_N can be estimated by applying the "belt model," which estimates the loss to plasma pressure based on the radial location and width of the tearing mode island [23]. Based on such analysis, Fig. 3(a2, b2, c2) illustrates the cost to plasma β_N due to the 4/2 tearing mode was 4-6% at t = 2.5 s for three cases in question. The 4/2 mode showed little change across the time interval of interest, so that one would expect little change in β_N between endpoints; this was, in fact, the case from experiment. However, the appearances of the 5/2 and 3/1 modes during neon and argon injection had a clearly harmful effect on β_N. For example, in the argon case, we estimate that by 4.0 s the 5/2 mode had reduced β_N by an additional ≈ 8% relative to the β_{N0} value at t = 2.5 s (Fig. 4(c2)); by t = 4.8 s, the presence of *both 5/2 and* 3/1modes (*minus* the 4/2 mode) had reduced β_N by ≈ 20% relative to β_{N0}. This predicted loss in plasma β_N is consistent with the data, where the experimentally determined drop in β_N by 4.8 s was ≈ 22% relative to β_{N0}. Similarly, for the neon case, the *predicted* reduction in plasma β_N between 2.5 s and 4.8 s was ≈ 21%, which was consistent with the *measured* reduction ≈ 18%. In this analysis, the impacts of each MHD mode to β_N reduction were treated as additive. Because power input, shaping, and other key plasma parameters were maintained constant throughout the times of interest, the fractional change in the energy confinement time to tearing mode onset would be very similar to that observed in β_N discussed above. Attempts to avoid the onset of these harmful 5/2 and 3/1 modes by reducing the argon or neon injection rates in order to provide a slower, more controlled plasma evolution appeared to only delay the onset of these modes.

Heat flux reduction experiments previously carried out at lower β_N were shown to reduce peak heat flux by a factor of two or three while maintaining β_N with minimal decrease in τ_E [5]. Deleterious tearing modes were less of a problem in those cases, which were operated further below the ideal MHD limits that characterized these equilibria. Thus far, reconstructing the key equilibria and their evolution with the required precision to understand what triggered the onset of these tearing modes has proved elusive. Moreover, a detailed model that would represent or predict the classical tearing instability index Delta-prime (Δ') for these highly shaped, high β_N plasmas, along with the value of Δ'-critical threshold value necessary to fully describe the tearing stability of these modes, is not available. Work on this topic, however, is continuing and will be the focus of a subsequent publication, if suitable models become available.

In these recent experiments, the susceptibility of high β_N DND plasmas to tearing modes during impurity injection complicates successful application of impurity seed-based approaches on DIII-D at moderate density. In future experiments, we plan to examine whether or not controlling the impurity profiles and hence the q-profile by adjusting the ECH deposition location can suppress (or at least reduce) the impact of these tearing modes [24].

3.2.1 *Radiating divertor*. Tearing modes are also found to be problematic when impurities are released into the private flux region (PFR) in the presence of deuterium flow. Here a crucial consideration in the success of a divertor design for high P_{IN}, high β_N plasmas rests in understanding the details of how impurities escape the divertor and build up in the core and the effect of this on tearing mode formation. Two otherwise identically-prepared high β_N plasmas differ by a 2-cm displacement in the radial location of the outer strike point (R_{OSP}), with the purple separatrix target closer to the upper outer pump, as shown in Fig. 4. Argon was injected into the PFR of the upper divertor, as shown, and all three cryo-pumps (two upper divertor and one lower divertor) were operational.

This small difference in R_{OSP} may have led to the clear difference in the rate of rise of argon in the core plasma shortly after argon impurities were injected into the PFR of the upper closed divertor. CER analysis indicates that the increase in core impurities was entirely due to argon, which is represented by the effective ion charge Z_{eff} (Fig 5(c)). Plasma β_N was not maintainable in the purple case having R_{OSP} closer to the pump, even with added power (Fig. 5(a, b). This influx was associated with tearing mode activity at t ≈ 3.7 s (Fig. 5d). Specific tearing mode activity in each of the two cases is shown in Fig. 6(a, b), where the "belt model" is again used to illustrate the effect that each mode has on τ_E degradation. While the 3/2 mode was present in both cases prior to impurity injection, the case with the more rapid increase in argon

produced more harmful tearing modes. From experimental measurements, we find that H_{98} decreased from 1.5 down to 0.9 in the purple case and down to 1.2 for the black case. These results show that even "minor" details of strike point placement inside the same closed divertor may lead to significant differences in maintaining a "clean" plasma. The reason such a relatively small variation in strike point location produces such a noticeable difference in argon "fuelling" of the main plasma is under investigation.

While tearing modes were present in lower power, lower β_N plasmas in previous work dealing with radiating divertor-based heat flux reduction, e.g., in Ref. 5, tearing modes have emerged as a serious issue in the high β_N plasmas considered here. Thus, minimizing the escape of seed impurities from the divertor should be a particularly important consideration where high β_N plasmas are involved.

3.3 Effect of divertor closure and magnetic balance on argon exhaust

Before one proceeds in assessing how changes in divertor closure and magnetic balance might affect argon exhaust, it is worthwhile to first demonstrate that the number of seed argon impurities injected into the DIII-D vessel is consistent with the number of argon particles being removed by the DIII-D pumps. In particular, the argon was removed by two of the cryo-pumps that were adjacent to the outer legs in either divertor. The upper inner pump was de-activated to ensure that argon was pumped only from locations with Penning gauges. Both double-null and single-null configurations were tested and argon was injected into the PFR of their primary divertor. Figure 7 is a plot of the total argon exhaust rate ($\Gamma_{\mathrm{AR-EXH}}$) versus the argon injection rate ($\Gamma_{\mathrm{AR-INJ}}$) and indicates good particle accountability for argon.

A more closed divertor had a measurable but modest effect on localizing where seed impurities in SNDs and DNDs were pumped. In this study, the upper outer divertor was considered as "closed" and the lower outer divertor as "open", i.e., without an inner baffle. For the DND cases, the level of argon that was injected into the PFR of the primary divertor of the upper-biased cases was pumped at a 10-20% higher rate than the same amount of argon that was injected into the PFR of the primary divertor in the more open (lower) divertor cases (Fig. 8a). This result was similar to the comparison of argon pumping rates for upper SND cases with lower SND cases, as shown in Fig. 8b.

3.4 Contribution of the inner pump to argon inventory control

Recent experiments on DIII-D have addressed the usefulness for active pumping of argon from the *inboard* side of upper-biased DND (dRsep = +3mm) and upper SND (dRsep = +21 mm) plasmas. Operating conditions were in the high-performance regime: P_{IN} = 12–15 MW, β_N = 3.3–3.6, H_{98} = 1.4-1.7, and the ion $\boldsymbol{B} \times \nabla B$ drift direction was toward the lower divertor. The results are summarized in Table 2 for the DND cases and in Table 3 for the SND cases. Argon was injected into the PFR of the upper divertor at low, medium, and high levels. For each injection level, we examined argon removal in two similarly-prepared plasmas, one in which the inner pump was activated and the other in which the inner pump was not activated.

In the DND case, the upper inner pump had virtually no role in argon removal at any of the argon injection levels (Table 2). The exhaust rate of the inner pump ($\boldsymbol{\Gamma_{\mathrm{AR-ID}}}$) was determined by inference, i.e., $\boldsymbol{\Gamma_{\mathrm{AR-ID}}} \approx \boldsymbol{\Gamma_{\mathrm{AR-INJ}}} - \boldsymbol{\Gamma_{\mathrm{AR-UOD}}} - \boldsymbol{\Gamma_{\mathrm{AR-LOD}}}$ where $\boldsymbol{\Gamma_{\mathrm{AR-UOD}}}$ and $\boldsymbol{\Gamma_{\mathrm{AR-LOD}}}$ are the exhaust rates for outer pump in the upper divertor and for the outer pump of the lower divertor, respectively. For each level of $\boldsymbol{\Gamma_{\mathrm{AR-INJ}}}$, $\boldsymbol{\Gamma_{\mathrm{AR-UOD}}}$ and $\boldsymbol{\Gamma_{\mathrm{AR-LOD}}}$ changed very little whether the inner pump was activated or not. This would be consistent with previous studies where argon injected into the private flux region of the upper divertor and ionized in the upper divertor would be preferentially swept away from the inner divertor target toward the outer target by $\boldsymbol{E_R} \times \boldsymbol{B}$-based particle flow [25,26]. Here, $\boldsymbol{E_R}$ is the radial electric field pointing into the PFR and $\boldsymbol{B}$ is the total magnetic field. Finally, in all cases we found that the inner pump removed $\approx 10\%$ of the deuterium gas which was injected into the main chamber.

Repeating these steps for the SND cases led to more complicated results (Table 3). For low $\boldsymbol{\Gamma_{\mathrm{AR-INJ}}}$, activating the inner pump made no difference in the argon pumped, similar to the DND result. For moderate $\boldsymbol{\Gamma_{\mathrm{AR-INJ}}}$, we raised the deuterium injection rate to ≈ 170 Torr l/s. With this, the case without inner divertor pumping detached, while the inner leg remained attached in the pumped case. What is particularly interesting in the attached case was that the inner pump now removed $\approx 25\%$ of the injected argon. Raising $\boldsymbol{\Gamma_{\mathrm{AR-INJ}}}$ further (but preserving the same deuterium gas puff rate) led to detachment at the inner divertor target, even with the inner divertor pump operating, along with a significant increase in both argon and carbon concentrations inside the main plasma. Under these detached conditions, $\boldsymbol{\Gamma_{\mathrm{AR-ID}}}$ returned to zero. Modelling these results with full particle drifts is ongoing. One hypothesis: (1) At low $\boldsymbol{\Gamma_{\mathrm{AR-INJ}}}$, $\boldsymbol{E_R} \times \boldsymbol{B}$-induced particle flow toward the outer divertor was dominant, (2) At moderate $\boldsymbol{\Gamma_{\mathrm{AR-INJ}}}$, the plasma was cooled but still attached, so that $\boldsymbol{E_R} \times \boldsymbol{B}$-driven flow was weakened sufficiently to allow some ionized argon in the PFR to diffuse over the upper inner target, and (3) At high $\boldsymbol{\Gamma_{\mathrm{AR-INJ}}}$, what was left of the inner divertor leg was no longer in contact with the inner divertor target adjacent to the inner pump entrance and $\boldsymbol{\Gamma_{\mathrm{AR-ID}}}$ returned to zero. Whether or not these SND plasmas are attached, deuterium exhaust by the inner pump accounted for $\approx 30\% - 40\%$ of the deuterium removed.

4. Discussion and conclusions

These recent studies have identified potential issues in reducing divertor heat flux in highly-powered, high performance DND and SND plasmas by using radiating mantle or radiating divertor-based solutions. Divertor and core modelling of these data is ongoing and will be reported on in a future follow-up paper.

The results presented in this paper indicate that minimizing seed impurity escape from the divertor is a *particularly* important consideration where high β_N plasmas are involved. Previous studies at lower power input and β_N found that significant divertor heat flux reduction, e.g., ≈ 3 times, was possible for DIII-D SNDs and DNDs by radiative methods, either by "seeding" the main plasma (radiating mantle) or indirectly by "seeding" the divertor directly. In the latter, some impurities could still escape the divertor and accumulate in the main chamber. In either approach, significant heat flux reduction and acceptable energy confinement and fuel dilution in the main plasma were achievable.

In recent attempts at lowering divertor heat flux at moderate density in high power, high β_N plasmas, impurity build-up in the main plasma resulted in significant dilution of the fuel specie (D^+) in the main plasma and particularly in its central region. In DIII-D, density limitations placed on ECH operation owing to the cut-off for X-mode polarization restricts the core density to low and moderate values (i.e., $\leq 5-6\times10^{19}\,m^{-3}$ or ≤ 0.6 of the Greenwald density). Hence, any reduction in divertor heat flux at higher power levels would demand higher impurity presence in both core and divertor, leading to an unacceptable fuel dilution. Thus, the radiating mantle method which would rely on significant radiated power from within the separatrix would not be an attractive solution for the high-performance plasmas discussed here. On the other hand, operating at higher density would ameliorate the need for a higher impurity presence in the main plasma. Introducing O-mode electron cyclotron heating in place of X-mode heating doubles the cut-off density and would allow access to the higher density (and more central electron cyclotron heating) needed to mitigate this fuel dilution problem.

A second serious obstacle to high power, high β_N plasma operation is confinement-killing tearing modes that accompany impurity seed injection. For radiating divertors, eliminating or at least moderating such harmful tearing mode activity by improving impurity confinement in the divertor would be an essential element in achieving successful heat flux reduction while minimizing loss in energy confinement. From that standpoint, methods relying on impurity accumulation in the edge or pedestal regions of the main plasma may run a serious risk of causing the onset of harmful tearing modes in high β_N plasmas; radiating mantle-based solutions may thus be at a disadvantage. Improving divertor closure was shown to be helpful in controlling impurity (argon) inventory, indicating that a more closed divertor would impede the escape of injected impurities, and would presumably ameliorate some of the concerns discussed in the above. In addition, a higher level of deuterium injection might create deuterium flow into the divertor that would also be helpful in preventing injected seed impurities from escaping into the plasma chamber and contaminating the plasma, i.e., "puff-and-pump" [1]. Finally, better understanding and control over q-profile evolution and how that affects tearing mode initiation could be the basis for another way to address this tearing mode issue. This would include modification to plasma shaping that would allow higher ideal stability limits, implying a higher β_N limit before harmful tearing modes begin to appear [27].

The value of an inner divertor pump for removing the seed argon in DNDs appears to be minimal. These results would have implications for future tokamak design, as, for example, the need for high field side particle exhaust in a double-null divertor-based design. For SND cases the value of the inner pump is complicated by the levels of divertor recycling and degree of divertor detachment. Modelling efforts are underway to better understand these results.

Acknowledgements

Work supported by the U.S. Department of Energy under DE-FC02-04ER54698[1], DE-AC02-09CH11466[2], DE-FG02-04ER54761[3], DE-AC52-07NA27344[4], DE-SC0013911[5], DE-AC05-06OR23100[6], and DE-NA0003525[7]. **Disclaimer:** This report was prepared as an account of work sponsored by an agency of the United States Government. Neither the United States Government nor any agency thereof, nor any of their employees, makes any warranty, express or implied, or assumes any legal liability or responsibility for the accuracy, completeness, or usefulness of any information, apparatus, product, or process disclosed, or represents that its use would not infringe privately owned rights. Reference herein to any specific commercial product, process, or service by trade name, trademark, manufacturer, or otherwise does not necessarily constitute or imply its endorsement, recommendation, or favoring by the United States Government or any agency thereof. The views and opinions of authors expressed herein do not necessarily state or reflect those of the United States Government or any agency thereof.

References

[1] M.R. WADE, et al., Nucl. Fusion **38** (1998) 1839.
[2] J.A. GOETZ, et al., J. Nucl. Mater. **266-269** (1999) 359.
[3] G.L. JACKSON, et al., Nucl. Fusion **42** (2002) 28.
[4] A. KALLENBACH, et al., J. Nucl. Mater. **337–339** (2005) 732.
[5] T.W. PETRIE, et al., J. Nucl. Mater. **363-365** (2007) 416.
[6] A. LOARTE, et al., Phys. Plasmas **18** (2001) 056105.
[7] C. GIROUD, et al., Nucl. Fusion **53** (2013) 113025.
[8] M. BERNERT, et al., Nucl. Mater. Energy **12** (2017) 111.

[9] T.H. OSBORNE, et al., Plasma Phys. Control. Fusion **42** (2000) A175.
[10] F. TURCO et al., Phys. Plasmas **22** (2015) 056113.
[11] C.C. PETTY, et al., Nucl. Fusion **56** (2016) 016016.
[12] T.C. LUCE, et al., Nucl. Fusion **41** (2001) 1585.
[13] M.R. WADE, et al.,Phys. Plasmas **8** (2001) 2208.
[14] T.W. PETRIE, et al., Nucl. Mater. Energy **19** (2019) 267.
[15] T.W. Petrie, et al., Nucl. Fusion **57** (2017) 086004.
[16] R. DUX, et al., Nucl. Fusion **39** (1999) 1509.
[17] S.P. HIRSHMAN and D.J. SIGMAR, Nucl. Fusion **21 (**1981) 1079.
[18] C. ANGIONI, et al., Nucl. Fusion **54** (2014) 083028.
[19] R. NEU, et al., Plasma Physics and Controlled Fusion **44** (2002) 811.
[20] H. HONG, et al., Nucl. Fusion **55** (2015) 063016.
[21] M.R. WADE et al., Phys. Plasmas **2** (1995) 2337.
[22] T.W. PETRIE, et al., Nucl. Materials and Energy, **12** (2017) 1141.
[23] Z. CHANG, J. D. CALLEN, Nucl. Fusion **30** (1990) 219.
[24] E. JOFFRIN, et al., Nucl. Fusion 54 (2014) 013011.
[25] T.W. PETRIE, et al., Nucl .Fusion **48** (2008) 045010.
[26] T.W. PETRIE, et al., Nucl. Fusion **49** (2009) 065013.
[27] A.D. Turnbull, et al., Nucl. Fusion **42** (2002) 917.

Tables and Figures

Table 1: *Fuel Dilution at Two Radial Locations for the Control Case, the Neon Case, and the Argon Case Discussed in Text.*

	n_D/n_e (ρ = 0.0)	n_D/n_e (ρ = 0.6)
Control [C only]	0.65	0.78
Neon [C + Ne]	0.20	0.30
Argon [Ar + C]	0.39	0.68

Table 2: *Argon Exhaust by Inner Pump in the Double-null Divertor*

	Γ_{AR-INJ} (Torr l/s)	Γ_{AR-UOD} (Torr l/s)	$\Gamma_{AAR-LOD}$ (Torr l/s)	Γ_{AR-ID} (Torr l/s)
w/o inner pump (attached)	1.08	0.92 (77%)	0.27 (23%)	----
w/ inner pump (attached)	1.08	0.93 (77%)	0.28 (23%)	$\cong 0^*$ ($\cong$ 0%)
w/o inner pump (attached)	1.63	1.43 (85%)	0.26 (15%)	----
w/ inner pump (attached)	1.63	1.40 (84%)	0.26 (16%)	$\cong 0^*$ ($\cong$ 0%)
w/o inner pump (attached)	2.40	2.14 (87%)	0.33 (13%)	----
w/ inner pump (attached)	2.40	2.16 (87%)	0.33 (13%)	$\cong 0^*$ ($\cong$ 0%)

Table 3: *Argon Exhaust by Inner Pump in the Single-null Divertor*

	Γ_{AR-INJ} (Torr l/s)	Γ_{AR-UOD} (Torr l/s)	$\Gamma_{AAR-LOD}$ (Torr l/s)	Γ_{AR-ID} (Torr l/s)
w/o inner pump (attached)	1.08	0.92 (81%)	0.27 (19%)	----
w/ inner pump (attached)	1.08	0.90 (81%)	0.28 (19%)	$\cong 0^*$ ($\cong$ 0%)
w/o inner pump (detached)	1.63	1.42 (89%)	0.17 (11%)	----
w/ inner pump (attached)	1.63	1.05 (64%)	0.18 (11%)	$\cong 0.40^*$ ($\cong$ 25%)
w/o inner pump (detached)	2.40	2.16 (92%)	0.19 (8%)	----
w/ inner pump (detached)	2.40	2.32 (93%)	0.18 (7%)	$\cong 0^*$ ($\cong$ 0%)

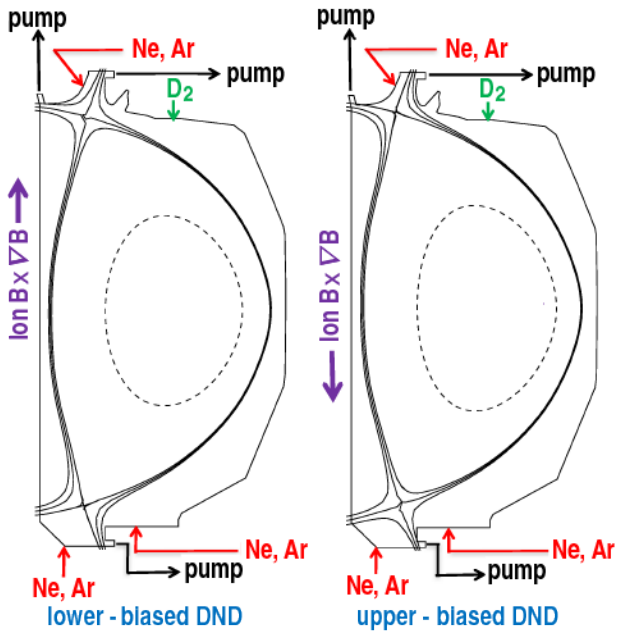

Fig. 1. *The unbalanced double-null plasma configurations used in this study can be biased either downward (a) or upward (b). The ion B x ∇B drift direction in either case is always away from the primary divertor. Particles are exhausted from cryopumps at three poloidal locations. Deuterium (D2) and the impurities (either neon or argon) can be injected from three poloidal locations, as shown.*

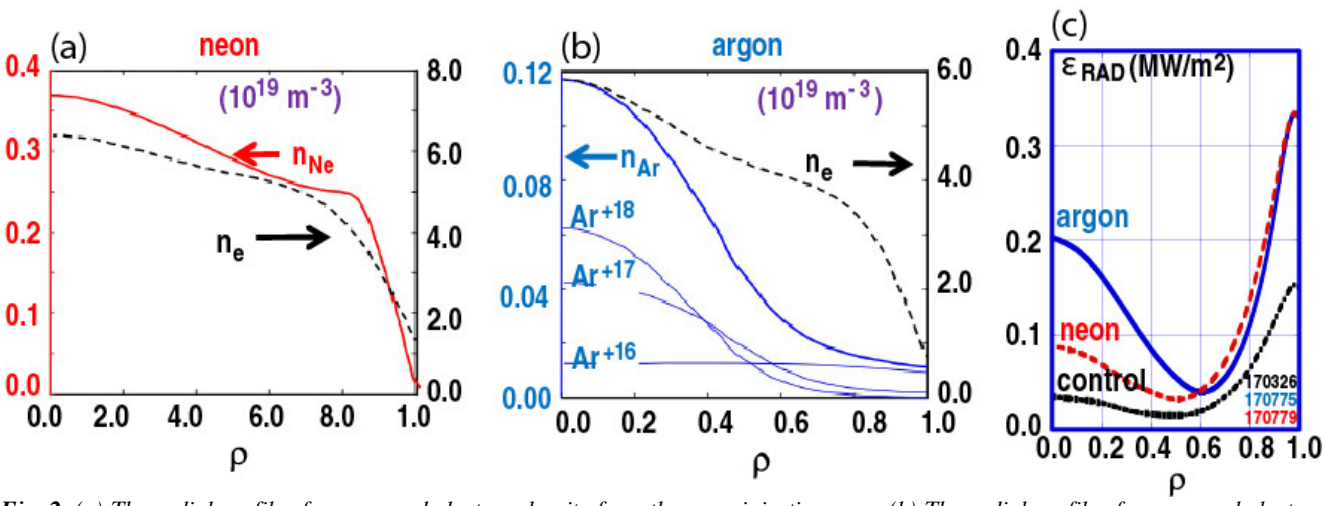

Fig. 2. *(a) The radial profiles for neon and electron density from the neon injection case. (b) The radial profiles for argon nd electron density from the argon injection case; included are the three ionization states of argon of most importance for* $\rho \leq 0.7$. *(c) The radial profile of the radiative emissivity for the control plasma case (dot-dashed in black), for the neon-seeded plasma case (dashed in red), and for the argon-seeded plasma case (solid in blue). The parameters:* $I_P = 1.0\ MA, q_{95} = 6, P_{IN} = 14.7\ MW, \beta_N = 3.5,\ H_{98} = 1.5,$ *and* $dRsep = -7\ mm$. *ECH deposition was at* $\rho = 0.45$.

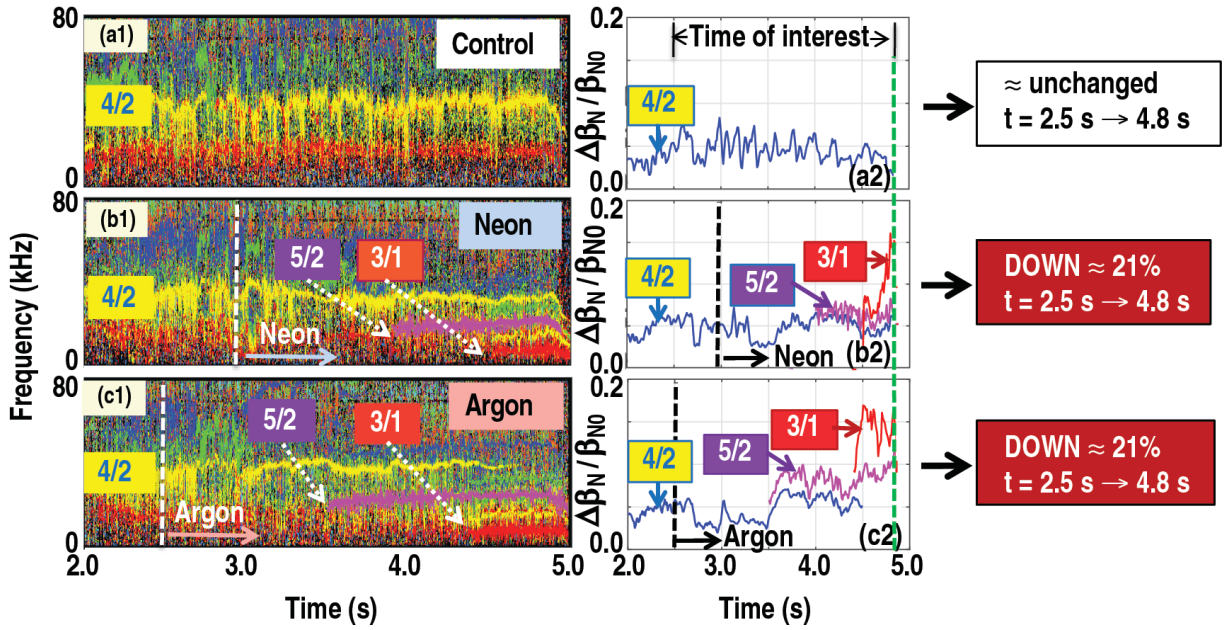

Fig. 3. *MHD activity during these high β_N hybrid shots are shown for the control shot (Fig. 3(a1), for the neon-seeded shot (Fig. 3(b1), and for the argon-seeded shot (Fig 3(c1). Each tearing mode should result theoretically in losses to stored energy or β_N [23]., and the fractional decrease in β_N from each mode is plotted in Fig. 3(a2), Fig. 3(b2), and Fig. 3(c2). Estimated cumulative loss over the time interval of interest for each of the three cases is shown in the third column.*

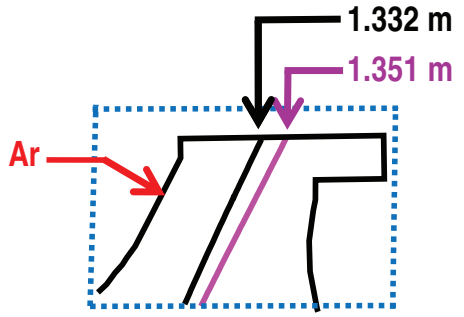

Fig. 4. *An enlarged cross-sectional view of the upper divertor showing the outer divertor strike points of two otherwise identically prepared, upper-biased double-null plasmas. Argon was injected into the private flux region. The results of Figures 5 and 6 are based on a modest difference in the radial strike point locations, i.e., ≈ 2cm. The operating parameters initially were: $H_{98} = 1.6$, $\beta_N = 3.3$. and dRsep = +3mm.*

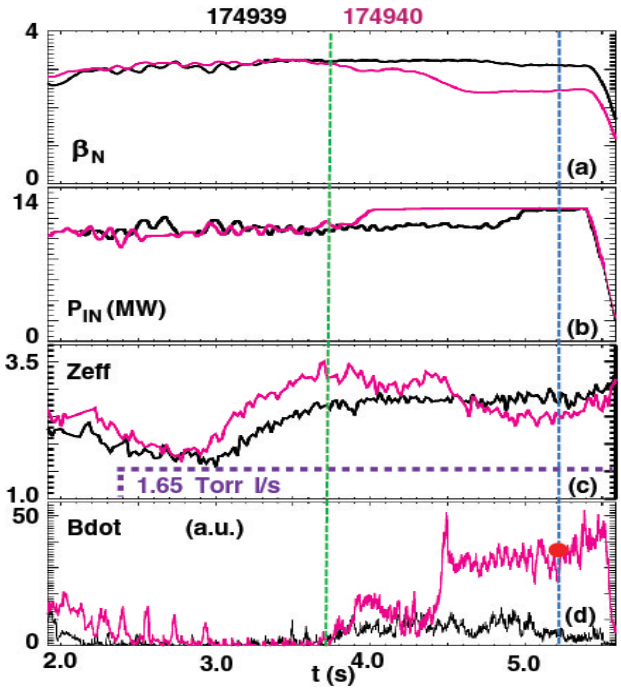

Fig. 5. *A small difference in outer strike point placement in a closed divertor produced a significant difference in the rate at which argon accumulated in the main plasma. (a) Normalized plasma beta β_N. (b) total power input P_{IN}, (c) Z_{eff}, and (d) a measure of MHD activity are shown. The vertical dashed line at 3.7 s indicates the time in which significant changes in MHD are observed, and the second vertical line indicates the time prior to the end of flattop.*

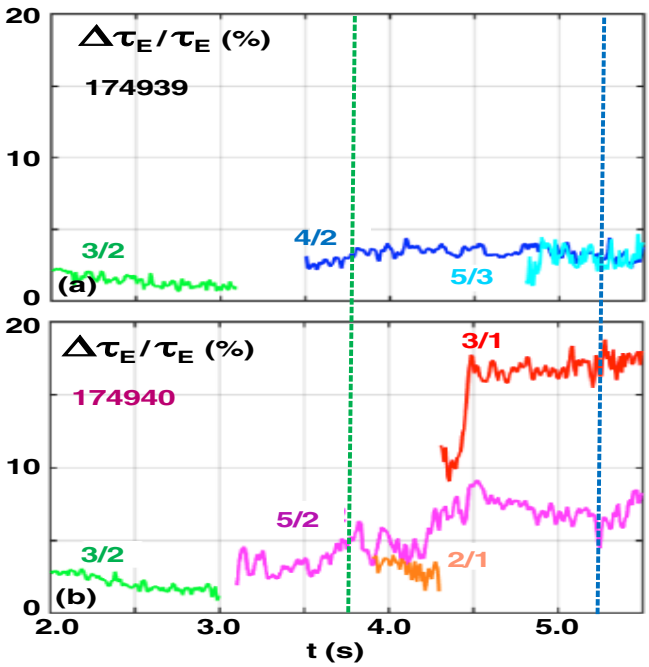

Fig. 6. *The change in energy confinement time with the onset of various tearing modes for the cases where the divertor strike point is farther from the pumping entrance (a) and closer to the pumping entrance (b).*

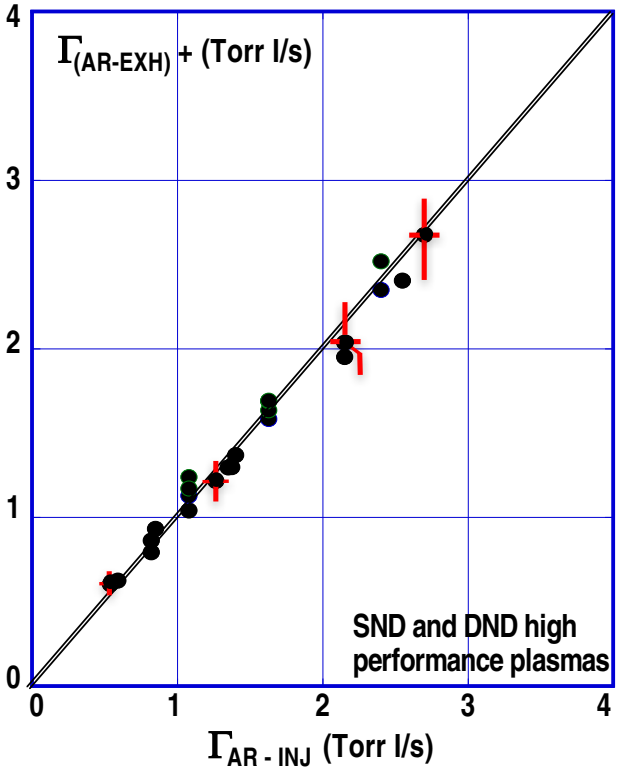

Fig. 7. *The argon injection rate ($\Gamma_{AR\text{-}INJ}$) is approximately equal to the total argon exhaust rate ($\Gamma_{AR\text{-}EXH}$), as measured by the two Penning gauges described in section 2. The upper inner cryo-pump was turned off. The data include both upper divertor-biased double-null and single-null configurations and lower divertor-biased SN and DN configurations. Error bars in red are added to selected data points.*

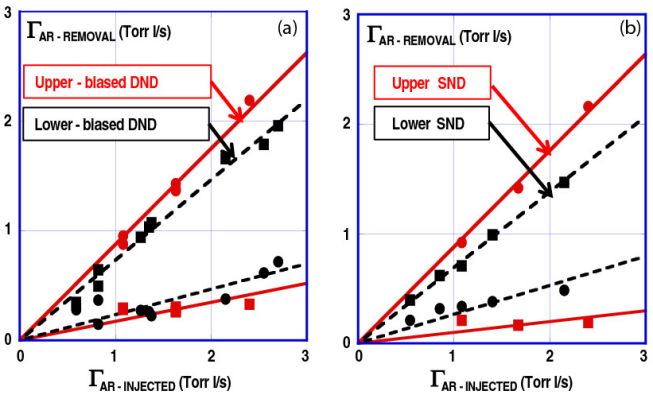

Fig. 8. *Argon removal rate for the upper and lower outer divertor pumps is shown as a function of the argon injection rate for both double-null (a) and single-null (b) configurations. Upper-biased plasmas are in red and lower-biased plasmas are in black. Circles represent pumping from the upper divertor and squares connote pumping from the lower divertor.*